THE JOURNAL OF BIOLOGICAL CHEMISTRY VOL. 284, NO. 13, pp. 8349–8358, March 27, 2009

Molecular Insight into the Synergism between the Minor Allele of Human Liver Peroxisomal Alanine:Glyoxylate Aminotransferase and the F152I Mutation*

Received for publication, November 26, 2008, and in revised form, January 8, 2009 Published, JBC Papers in Press, January 20, 2009, DOI 10.1074/jbc.M808965200

Barbara Cellini[‡], Riccardo Montioli[‡], Alessandro Paiardini[§], Antonio Lorenzetto[‡], and Carla Borri Voltattorni[‡1]

From the [‡]Dipartimento di Scienze Morfologico-Biomediche, Sezione di Chimica Biologica, Facoltà di Medicina e Chirurgia, Università degli Studi di Verona, Strada Le Grazie, 8, 37134 Verona, Italy and the [§]Dipartimento di Scienze Biochimiche "A. Rossi Fanelli" and Centro di Biologia Molecolare del Consiglio Nazionale delle Ricerche, Università "La Sapienza", 00185 Rome, Italy

Human liver peroxisomal alanine:glyoxylate aminotransferase (AGT) is a pyridoxal 5′-phosphate (PLP)-dependent enzyme that converts glyoxylate into glycine. AGT deficiency causes primary hyperoxaluria type 1 (PH1), a rare autosomal recessive disorder, due to a marked increase in hepatic oxalate production. Normal human AGT exists as two polymorphic variants: the major (AGT-Ma) and the minor (AGT-Mi) allele. AGT-Mi causes the PH1 disease only when combined with some mutations. In this study, the molecular basis of the synergism between AGT-Mi and F152I mutation has been investigated through a detailed biochemical characterization of AGT-Mi and the Phe^{152} variants combined either with the major (F152I-Ma, F152A-Ma) or the minor allele (F152I-Mi). Although these species show spectral features, kinetic parameters, and PLP binding affinity similar to those of AGT-Ma, the Phe^{152} variants exhibit the following differences with respect to AGT-Ma and AGT-Mi: (i) pyridoxamine 5′-phosphate (PMP) is released during the overall transamination leading to the conversion into apoenzymes, and (ii) the PMP binding affinity is at least 200–1400-fold lower. Thus, Phe^{152} is not an essential residue for transaminase activity, but plays a role in selectively stabilizing the AGT-PMP complex, by a proper orientation of Trp^{108}, as suggested by bioinformatic analysis. These data, together with the finding that apoF152I-Mi is the only species that at physiological temperature undergoes a time-dependent inactivation and concomitant aggregation, shed light on the molecular defects resulting from the association of the F152I mutation with AGT-Mi, and allow to speculate on the responsiveness to pyridoxine therapy of PH1 patients carrying this mutation.

The human liver peroxisomal alanine:glyoxylate aminotransferase (AGT)[2] is a pyridoxal 5′-phosphate (PLP)-dependent enzyme of clinical relevance in that its deficiency is associated with primary hyperoxaluria type 1 (PH1), a rare genetic disease characterized by progressive renal failure due to accumulation of insoluble calcium oxalate (1). In the peroxisomes of normal human hepatocytes, AGT is responsible for conversion of glyoxylate to glycine. This can be considered to be a detoxification reaction because its disfunction in PH1 allows glyoxylate to build up and to convert to oxalate. The two most common normal intragenic haplotypes of the AGT gene (*AGXT*) are referred to as the major and minor alleles (AGT-Ma and AGT-Mi). AGT-Mi differs from AGT-Ma by two coding sequence polymorphisms (P11L and I340M) and a non-coding duplication in intron 1. These polymorphisms have no clinical significance on their own, but they enhance the deleterious effects of several common PH1 mutations that occur on the same allele (2). This combination generates polymorphic variants characterized by impairments in the stability, localization, and/or rate of dimerization (2).

The 2.5-Å resolution structure of human AGT in complex with the competitive inhibitor aminooxyacetic acid reveals that the enzyme is a dimer. Each monomer consists of a N-terminal arm (residues 1–21), a large domain (residues 22–282), and a smaller C-terminal domain (residues 283–392). One PLP cofactor is bound per subunit and is present in a Schiff base linkage to the active site lysine, Lys^{209}. Analysis of this structure has allowed the rationalization of some, but not all, of the effects of disease-specific mutations (3). A detailed study of the reaction catalyzed by wild-type AGT was recently done. Kinetic, spectroscopic, and computational methods have demonstrated that (i) the enzyme is highly specific for catalyzing glyoxylate to glycine processing, (ii) pyridoxamine 5′-phosphate (PMP) remains bound to the enzyme during the catalytic cycle, and (iii) the AGT-PMP complex displays a reactivity toward keto acids higher than that of apoAGT in the presence of PMP (4).

Notwithstanding an increase in understanding the functional synergism between the P11L and I340M polymorphism and the PH1-specific mutations, one of the most intriguing biochemical questions is why and how this synergism occurs. Recent "*in vitro*" and "*in vivo*" studies have established that AGT-Mi is less stable and active than AGT-Ma (5). It has also been reported that some variants (G170R, I244T, F152I) encoded on the background of the minor allele have reduced steady-state protein levels, and it has been hypothesized that this reduction could be largely due to protein destabilization

* This work was supported by grants from the Oxalosis and Hyperoxaluria Foundation (OHF) and Ministero dell'Università e della Ricerca (PRIN 2007) (to C. B. V.). The costs of publication of this article were defrayed in part by the payment of page charges. This article must therefore be hereby marked "*advertisement*" in accordance with 18 U.S.C. Section 1734 solely to indicate this fact.

[1] To whom correspondence should be addressed. Tel.: 39-045-8027-175; Fax: 39-045-8027-170; E-mail: carla.borrivoltattorni@univr.it.

[2] The abbreviations used are: AGT, alanine:glyoxylate aminotransferase; PLP, pyridoxal 5′-phosphate; PMP, pyridoxamine 5′-phosphate; HPLC, high pressure liquid chromatography; PH1, primary hyperoxaluria type 1; CASTp, computed atlas of surface topography of proteins; AGT-Mi, AGT-minor; AGT-Ma, AGT-major.

(5). However, although PLP seems to stabilize, even to a different extent, both AGT-Ma and AGT-Mi, it does not appear to have any stabilizing effect on the PH1-causing variants (5).

F152I is one of the mutations that co-segregate and functionally interact with the P11L and I340M polymorphisms of the minor allele (2). PH1 patients carrying this mutation show the presence of mitochondrial AGT in addition to soluble peroxisomal AGT (6). The effect of this substitution on the minor allele cannot be understood in structural terms. Phe[152] is not located at the active site of the enzyme. Its side chain fills up a hydrophobic hollow limited by a β-sheet containing Phe[152] and the helix 5 whose N-terminal residue is Trp[108], the PLP-sandwiching residue. Up to now the molecular defect of the F152I mutation associated with the minor allele (F152I-Mi) has not yet been identified.

The present study is aimed at understanding the molecular origin of the PH1-associated F152I-Mi variant. For this purpose, we have carried out a detailed characterization of the recombinant purified AGT-Mi, F152-Mi (F152I-Mi), and F152-Ma (F152I-Ma, F152A-Ma) variants. Although these enzymatic species display spectroscopic features, kinetic parameters, and PLP binding affinity comparable with those of AGT-Ma, F152I mutants exhibit substantial differences with respect to AGT-Ma or AGT-Mi. In fact, whereas PMP remains tightly bound to the protein during the L-alanine half-transamination and the overall transamination of both AGT-Ma and AGT-Mi, it is released from the Phe[152] variants. This result is consistent with the finding that mutation at position 152 leads to at least a 200–1400-fold reduction of the binding affinity of PMP. These data strongly suggest a role of Phe[152] in the selective stabilization of PMP binding in AGT. Moreover, among all the holo and apo enzymatic species examined in the present study, F152I-Mi in the apo form is the only one that displays a gradual and consistent decrease of transaminase activity upon incubation for 3 h at 37 °C. The inactivation is dependent on protein concentration and parallels formation of insoluble high molecular weight aggregates. These results, together with the bioinformatic analysis of the putative binding mode of PMP in Phe[152] mutants, allows us to identify for the first time the structural and functional molecular defects resulting from the combination of the F152I mutation with the minor allele. The possible molecular basis of the responsiveness to pyridoxine therapy of PH1 patients bearing this mutation has also been proposed.

EXPERIMENTAL PROCEDURES

Materials—PLP, PMP, L-alanine, glyoxylate, pyruvate, rabbit muscle L-lactic dehydrogenase, and isopropyl β-D-thiogalactoside were all purchased from Sigma. All other chemicals were of the highest purity available.

Site-directed Mutagenesis—AGT-His mutants were constructed using the QuikChange site-directed mutagenesis kit (Stratagene). The oligonucleotides used for mutagenesis are as follows: P11L forward primer, 5′-GCTGCTGGTGACCCCCCTCAAGGCCCTGCTCAAGC and its complement; I340M forward primer, 5′-CATCGTCAGCTACGTCATGGACCACTTCGACATTG and its complement; F152I forward primer, 5′-CCAGTGCTGCTGATCTTAACCCACGGGG and its complement; F152A forward primer, 5′-AAGCCAGTGCTGCTGGCCTTAACCCACGGGGAG and its complement. The underlined codons are for mutated amino acids. All mutations were confirmed by DNA sequence analysis.

Expression and Purification—Wild-type and mutant enzymes in their His-tagged form associated with the major or minor allele were expressed and purified as previously reported (4).

The apo forms of the mutants were prepared as already described (4). The protein concentration in the AGT samples was determined by absorbance spectroscopy using an extinction coefficient of $9.4 \times 10^4\ \text{M}^{-1}\ \text{cm}^{-1}$ at 280 nm (4). The PLP content of the mutants was determined by releasing the coenzyme in 0.1 M NaOH and by using $\epsilon = 6600\ \text{M}^{-1}\ \text{cm}^{-1}$ at 388 nm.

Enzyme Assays—Pyruvate formation was measured either by the spectrophotometric assay using the coupled lactate dehydrogenase system (7) or, when the pyruvate concentration was lower than 100 μM, the more sensitive HPLC method after derivatization with 2,4-dinitrophenylhydrazine as previously described (8). The latter method has also been used for determination of glyoxylate consumption. Kinetic parameters for the pair alanine/glyoxylate of AGT-Mi, F152I-Mi, F152I-Ma, and F152A-Ma were determined in the presence of 150 μM PLP by varying the substrate concentrations at a fixed saturating co-substrate concentration. Data were fitted to the Michaelis-Menten equation. The detection and quantification of PLP and PMP were performed using the HPLC procedure reported previously (9).

Equilibrium Dissociation Constants for Mutants of PLP and PMP—The equilibrium dissociation constant for PLP, $K_{D(\text{PLP})}$, from AGT-Mi, F152I-Mi, F152I-Ma, and F152A-Ma was determined by measuring the quenching of the intrinsic fluorescence of apoenzymes (0.1 μM) in the presence of PLP at a concentration range 0.01–10, 0.01–5, 0.002–5, and 0.02–4 μM, respectively.

The equilibrium dissociation constant for PMP, $K_{D(\text{PMP})}$, for F152I-Mi, F152I-Ma, and F152A-Ma was determined by CD spectrometric titration at 290 nm of the apo forms at a concentration of 6–10 μM in the presence of PMP at concentration ranges of 5–300, 5–240, and 22–250 μM, respectively. All these experiments were carried out in 100 mM potassium phosphate buffer, pH 7.4. The $K_{D(\text{PLP})}$ and $K_{D(\text{PMP})}$ values for the mutant-coenzyme complexes were obtained using Equation 1,

$$Y = Y_{\text{max}} \frac{[E]_t + [\text{Pyx}]_t + K_{D(\text{Pyx})} - \sqrt{([E]_t + [\text{Pyx}] + K_{D(\text{Pyx})})^2 - 4[E]_t[\text{Pyx}]_t}}{2[E]_t} \quad \text{(Eq. 1)}$$

where $[E]_t$ and $[\text{Pyx}]_t$ represent the total concentrations of the mutant and PLP or PMP, respectively, Y refers to either the intrinsic quenching or the 290-nm dichroic signal changes at a Pyx_t concentration, [Pyx], and Y_{max} refers to the aforementioned changes when all enzyme molecules are complexed with coenzyme.

A $K_{D(\text{PMP})}$ value cannot be determined for both AGT-Ma and AGT-Mi by CD or fluorescence spectroscopy given that the enzyme concentration required far exceeds the $K_{D(\text{PMP})}$ value.

However, a lower limit value has been estimated as follows: AGT-PMP complex at 0.1 μM concentration was incubated at 25 °C for 2 h, then the mixtures were subjected to filtration through a Centricon-30 device and the amount of PMP was measured in the filtrates by HPLC analysis. The behavior of AGT-PMP at a concentration lower that 0.1 μM cannot be examined because 0.1 μM is the detection limit of PMP.

Pre-steady-state Analysis by UV-visible Spectrophotometry—The reaction of holoF152A (6 μM) with various concentrations of L-alanine (10–150 mM) as well as the reaction of F152A in the apo form (10 μM) preincubated overnight with 250 μM PMP and various concentrations of glyoxylate (0.15–2.5 mM) were carried out in 100 mM phosphate buffer, pH 7.4, at 25 °C in a total volume of 120 μl. In each case, absorbance spectra (500) from 250 to 550 nm were recorded on a J&M Tidas 16256-diode array detector (Molecular Kinetics) using a BioLogic SFM300 instrument. The dead-time was 3.6 ms at a flow velocity of 12 ml/s. The rate constants measured by following the changes at 420 and/or 330 nm were determined by non-linear regression to Equation 2,

$$A_t = A_\infty + \Delta A e^{(-k_{obs}t)} \quad \text{(Eq. 2)}$$

where A_t is the absorbance at time t, ΔA is the amplitude of the phase, k_{obs} is the observed rate constant, and A is the final absorbance. Data were analyzed using the Biokine 4.01 (BioLogic) software provided with the instrument. The k_{max} and apparent K_m values for the half-reaction were determined by plotting the observed rate constants *versus* substrate concentrations and fitting the data to Equation 3.

$$k_{obs} = \frac{k_{max}[S]}{K_m^{app} + [S]} \quad \text{(Eq. 3)}$$

Size Exclusion Chromatography—Chromatography experiments were performed on a Sephacryl S-300 column (GE Healthcare) coupled to an AKTA FPLC system (Amersham Biosciences), equipped with a UV detector. The column was preequilibrated with 100 mM potassium phosphate buffer, pH 7.4, before injections. Protein concentration was in the range 0.25–1 μM, and the flow rate was 1 ml/min.

Thermostability—The thermal stability experiments of AGT-Ma, AGT-Mi, F152I-Mi, F152I-Ma, and F152A-Ma in the holo and apo forms were performed as follows: 1) holoenzymes in the presence of 100 μM PLP or apoenzymes, both at a concentration of 0.16 μM, were preincubated for 10 min at different temperatures ranging from 25 and 80 °C. Following preincubation, and, upon addition of 100 μM PLP to the solution of apoenzymes, samples were placed on ice for 45 min; 2) holoenzymes in the presence of 100 μM PLP or apoenzymes, both at a concentration ranging from 0.25 to 1 μM, were incubated at 37 °C over a period of 180 min. Aliquots were removed at different times and, upon addition of 100 μM exogenous PLP only to the solutions of apoenzymes, placed on ice for 45 min. In both types of experiments (1 and 2), samples were assayed for transaminase activity at 25 °C in the presence of exogenous PLP as specified above.

Molecular Modeling—The three-dimensional coordinates of the human AGT (Protein Data Bank code 1H0C) (3) in its dimeric assembly and with PLP bound in the internal aldimine configuration were initially used as a starting point to generate the PMP bound forms of the enzyme, by means of the BUILDER package from InsightII (V.2005, MSI, Los Angeles, CA). PMP was initially positioned into the active site following the binding mode observed for PLP in the crystal structure of PDB 1H0C. Then, energy minimization was carried out to energetically relax the complex. After an initial minimization performed on the whole system to allow added hydrogens to adjust to the crystallographically defined environment, and fixing all the other atom types, a gradually decreasing tethering force using steepest descents and conjugated gradients was applied to the whole system, until the latter was totally relaxed. The maximum derivative achieved was 0.0001 kcal mol^{-1} $Å^{-1}$. Only PMP, main chain, and side chains of every residue comprised in a sphere of 20 Å from the PMP were free to move during the simulation. All minimizations were carried out using the Cff91 forcefield, as implemented in Discover 2.9 and the Analysis package of InsightII. Active site structural water molecules, which were observed in PDB 1H0C, were not considered. Nonbond terms were truncated at 40 Å (smoothing from 36 Å), with a switching function for van der Waals and electrostatic terms. Because the other water molecules were not explicitly included, a distance-dependent dielectric was used throughout the minimizations. A similar protocol was applied to explore the potential energy surface of Trp^{108} within the active site pocket (see below).

After PMP minimization, the BIOPOLYMER package from InsightII was used to mutate Phe^{152} of the crystal structure of human AGT, to obtain the single F152I and F152A mutants. The identification and analytical computation of area/volume of cavities in the wild-type and *in silico* mutated forms of AGT was performed by means of the CASTp tool (available at sts-fw.bioengr.uic.edu/castp/index.php) (10). CASTp (Computed Atlas of Surface Topography of proteins) is a tool aiming to provide a quantitative characterization of interior cavities and surface pockets of proteins. In CASTp, cavities are defined as buried unfilled empty space inside the protein. Heteroatoms that are inaccessible to solvent molecules from outside were ignored during the computation.

The energy-minimized structure was then used to explore the potential energy surface of Trp^{108} within the active site pocket. To this purpose, starting from each rotameric position of Trp, each different conformation of the complex was subjected to energy minimization and molecular dynamics. All atoms of the structure were fixed, except those interacting with the side chain at a cutoff distance of 6 Å, during its rotation. Dynamic simulation was performed for 10,000 steps at 300 K, after a 100 steps equilibration at the same temperature. The total energy of the system was monitored for the entire simulation. The Cff91 forcefield, a distance-dependent dielectric constant, and a 1-fs time step were used during the simulation. Each conformation was finally relaxed by 1000 steepest descents minimization steps.

Spectrophotometric Measurements—Absorption measurements were made with a Jasco V-550 spectrophotometer. Fluorescence spectra were taken with a Jasco FP-750 spectrofluorometer using 5 nm excitation and emission bandwidth at a

TABLE 1
Steady-state kinetic parameters of AGT-Ma, AGT-Mi, and variants (Fig. 2) for the pair alanine-glyoxylate

Enzyme	Substrate	Cosubstrate	k_{cat}	K_m L-alanine	K_m glyoxylate	k_{cat}/K_m
			s^{-1}	mM		s^{-1} mM^{-1}
AGT-Ma	L-Alanine	Glyoxylate	45 ± 2[a]	31 ± 4[a]		1.4 ± 0.2[a]
	Glyoxylate	L-Alanine	45 ± 3[a]		0.23 ± 0.05[a]	196 ± 44[a]
AGT-Mi	L-Alanine	Glyoxylate	33 ± 5	28 ± 2		1.2 ± 0.2
	Glyoxylate	L-Alanine	37 ± 1		0.22 ± 0.01	168 ± 8
F152I-Mi	L-Alanine	Glyoxylate	33.6 ± 0.3	41 ± 1		0.82 ± 0.02
	Glyoxylate	L-Alanine	40 ± 2		0.25 ± 0.03	160 ± 21
F52I-Ma	L-Alanine	Glyoxylate	35 ± 1	37 ± 1		0.95 ± 0.04
	Glyoxylate	L-Alanine	39 ± 1		0.28 ± 0.04	139 ± 20
F152A-Ma	L-Alanine	Glyoxylate	21.2 ± 0.6	46 ± 3		0.46 ± 0.03
	Glyoxylate	L-Alanine	22.6 ± 0.3		0.34 ± 0.02	66 ± 4

[a] From Ref. 4.

protein concentration of 1 or 5 μM. Spectra of blanks, that is, samples containing all components except the enzyme, were taken immediately before the measurements of samples containing protein. CD spectra were obtained using a Jasco J-710 spectropolarimeter with a thermostatically controlled compartment at 25 °C. For far-UV measurements, the protein concentration was 1 μM with a path length of 0.1 cm. For near-UV measurements, the protein concentration varied from 1 to 10 μM in a cuvette with a path length of 1 cm. Routinely, three spectra were recorded at a scan speed of 50 nm min^{-1} with a bandwidth of 2 nm and averaged automatically, except where indicated. Secondary structure content was calculated from far-UV spectra using the CD spectra deconvolution software (11).

Data Analysis—The kinetic and thermostability experiments were performed at least in duplicate and in each case the S.E. was less than 5%. All data analysis was performed by non-linear regression curve fitting using Origin® 7.03 (Origin Lab) and the errors indicated result from fitting to the appropriate equation.

RESULTS AND DISCUSSION

The aim of this work was the study of the molecular basis of the functional synergism between the P11L and I340M polymorphisms and the F152I mutation giving rise to PH1 disease. To this purpose, we cloned, expressed, purified, and characterized AGT-Mi and F152 variants combined either with the major or the minor allele. The purified natural and unnatural mutants were homogenous as indicated by a single band detected on SDS-PAGE with a mobility identical to that of the corresponding wild-type. Generally, yields of AGT-Mi and mutant enzymes after the standard purification procedure were comparable with the yield of AGT-Ma. However, the yield of F152I-Mi was only about 25% that of AGT-Ma. There were no detectable differences between the far-UV CD spectra of AGT-Ma and those of the mutant enzymes. This suggests that mutations do not affect the composition of secondary structure elements.

AGT-Mi, F152I-Mi, and F152I-Ma: Spectroscopic and Kinetic Properties—As isolated, AGT-Mi, F152I-Mi, and F152I-Ma bind 2 mol of PLP per dimer and display absorbance, dichroic, and fluorescence features identical to those of AGT-Ma (4) (data not shown). The steady-state kinetic parameters of AGT-Mi, F152I-Mi, and F152I-Ma for the pair alanine-glyoxylate measured in the presence of exogenous PLP are listed in Table 1. The catalytic efficiency of AGT-Mi is reduced by only 0.8-fold as compared with that of AGT-Ma. Moreover, the k_{cat}/K_m values of F152I-Mi and F152I-Ma are reduced by 1–1.4-fold with respect to those of AGT-Mi. Again, as shown in Table 2, whereas the $K_{D(PLP)}$ value of AGT-Mi is identical to that of AGT-Ma, those of F152I-Mi and F152I-Ma are similar to each other and slightly lower than those of AGT-Ma and AGT-Mi. Taken together, these data indicate that the F152I mutation when in combination with either the major or the minor allele does not appear to significantly affect either the spectroscopic and catalytic properties of the enzyme or the PLP binding affinity. Therefore, Phe[152] is not an essential residue for transaminase activity.

TABLE 2
Equilibrium binding constants for AGT-Ma, AGT-Mi, and Phe[152] mutants of PLP and PMP

Enzyme	$K_{D(PLP)}$	$K_{D(PMP)}$
	μM	
AGT-Ma	0.27 ± 0.03[a]	<0.1[a]
AGT-Mi	0.26 ± 0.02	<0.1
F152I-Mi	0.085 ± 0.006	19 ± 4
F152I-Ma	0.06 ± 0.01	22 ± 3
F152A-Ma	0.20 ± 0.03	142 ± 22

[a] From Ref. 4.

To acquire more detailed information on the kinetic process of AGT-Mi, F152I-Mi, and F152I-Ma, absorbance and CD spectral changes occurring during their half-transamination reactions have been monitored and compared with those previously reported for AGT-Ma. Spectral changes during L-alanine half-transamination catalyzed by AGT-Mi are qualitatively identical to those of AGT-Ma (4). They only consist in the immediate disappearance of both the 420-nm absorbance band and the 429-nm dichroic band, and the concomitant appearance of a 330-nm absorbance band and the positive dichroic signals at 320 and 260 nm, as well as an increase of the dichroic bands in the 290-nm region. Furthermore, like in AGT-Ma (4), PMP remains tightly bound to AGT-Mi during the L-alanine half-transamination. When L-alanine (500 mM) was added to holoF152I-Mi or holoF152I-Ma (6 μM) the immediate absorbance and CD spectral changes are identical to those of AGT-Ma or AGT-Mi. However, unlike for AGT-Ma or AGT-Mi, we could observe that with time the 330-nm absorbance band shifts to 326 nm and increases, and the positive dichroic signals (320, 260, and 290 nm) decrease (Fig. 1, *A* and *B*). After 4 h of reaction of F152I-Mi or F152I-Ma with L-alanine, the solution was filtered through a Centricon-30 device. HPLC analysis of the filtrate reveals not only the presence of pyruvate but also

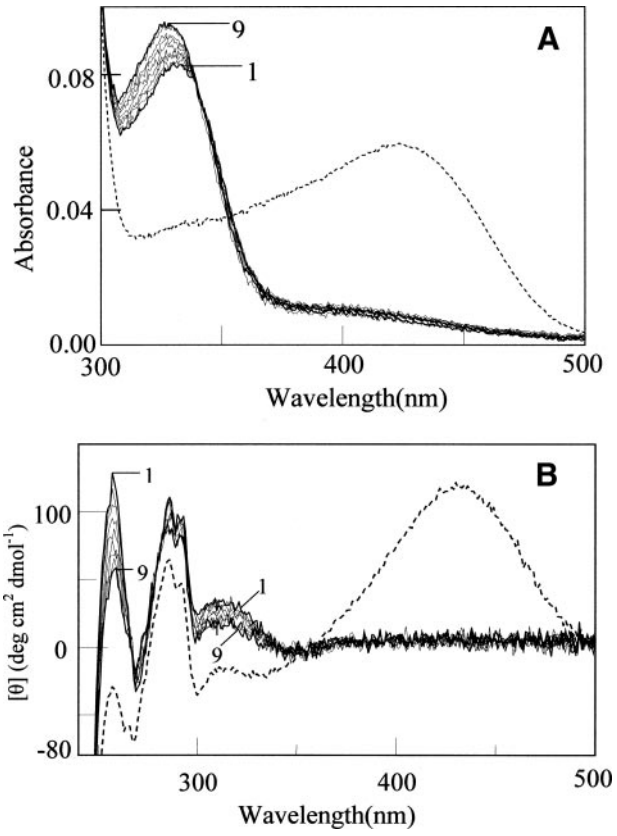

FIGURE 1. **Absorption and CD spectral changes upon addition of L-alanine to F152I-Mi.** *A*, absorption spectra of 6 μM F152I-Mi (- - -) and of the enzyme plus 500 mM L-alanine (—) immediately (*line 1*) and after 0.6, 3, 8, 14, 26, 34, 60, 100, and 180 min (*line 9*). *B*, CD spectra of 5 μM F152I-Mi (- - -) and the enzyme plus 500 mM L-alanine (—) immediately (*line 1*) and after 8, 15, 23, 48, 68, 100, 125, and 206 min (*line 9*). In each case, the buffer used was 100 mM potassium phosphate, pH 7.4.

that of PMP in an amount equal to ~60% of the original PLP content. The remaining aliquot of PMP was detected in the supernatant of the retentate after denaturation. These data indicate that, unlike for AGT-Mi and AGT-Ma, a large amount of PMP formed during the L-alanine half-transamination does not remain bound to F152I-Mi and F152I-Ma. Upon addition of glyoxylate or pyruvate to apoAGT-Mi, apoF152I-Mi, or apoF152I-Ma preincubated with 200 μM PMP, a recovery of the absorbance and dichroic features of the original holoenzymes was immediately seen, which is like that seen for AGT-Ma.

The different behavior observed during the L-alanine half-transamination by F152I-Mi and F152I-Ma with respect to AGT-Mi (or AGT-Ma) is validated by the values of their $K_{D(PMP)}$ (Table 2). It has not been possible to determine a $K_{D(PMP)}$ value for AGT-Mi and AGT-Ma. However, the finding that, upon filtration through a Centricon-30 device of these enzymatic species in the PMP form at a concentration of 100 nM, no PMP could be detected in both the filtrates allows us to establish that the $K_{D(PMP)}$ for both AGT-Ma and AGT-Mi should be <0.1 μM (see "Experimental Procedures"). Therefore, although these data do not allow to establish if the P11L and I340M substitutions affect the PMP binding affinity, they clearly indicate that the additional mutation at position 152 either on the major or minor allele causes an at least 200-fold decrease in PMP binding affinity. The finding that mutations at position 152 of AGT cause an increase in $K_{D(PMP)}$ without significantly affecting the $K_{D(PLP)}$ strongly suggests that the energy of AGT-PMP has been increased selectively compared with that of AGT-PLP. This points out a different defect of the F152I variants with respect to that of the previously studied G82E variant. In the latter, both PLP and PMP binding states were significantly altered resulting in a dramatic reduction of the overall catalytic activity (4).

Neither the inspection of the crystal structure of AGT nor the steady-state kinetic parameters measured in the presence of exogenous PLP can suggest an obvious role played for Phe[152] in catalysis. Nevertheless, we decided to monitor the status of PMP (free and/or bound) during the overall transamination catalyzed by AGT-Ma, AGT-Mi, and F152I variants in the absence of exogenous PLP. These enzymatic species at a concentration of 2.6 μM (*i.e.* at a concentration ~10-fold higher than their $K_{D(PLP)}$ values) were incubated at body temperature (37 °C) in the presence of 0.5 M L-alanine and 3 mM glyoxylate. Aliquots were withdrawn from the reaction mixtures at various times, and the time courses of coenzymes content, pyruvate formation, and glyoxylate consumption were determined. In all cases glyoxylate is rapidly consumed and concomitantly pyruvate is produced, and PMP increases at the expense of the original PLP content of the enzyme. The PLP into PMP conversion for both AGT-Ma and AGT-Mi occurs rapidly and in a monophasic manner reaching a PMP/PLP ratio of about 0.4 (Fig. 2*A*). In contrast, the conversion of the original PLP content of F152I-Mi and F152I-Ma into PMP proceeds for several hours. At 3 h the ratio PMP/PLP is 1.2. The best fit for both increase in PMP and decrease in PLP of the F152I-Mi and F152I-Ma mutants was to a two-exponential process: the rate constants for the two phases are 2.6 ± 0.3 and 0.014 ± 0.003 min^{-1} for F152I-Mi, and 3.1 ± 0.5 and 0.027 ± 0.002 min^{-1} for F152I-Ma (Fig. 2*B*). If the overall transamination of AGT-Ma, AGT-Mi, and F152I variants under the above experimental conditions is followed by monitoring CD changes in the near-UV region, we observe in any case the immediate appearance of a positive dichroic signal at 260 nm, typical of the AGT-PMP complex (4). However, whereas this signal remains almost unaltered with time for both AGT-Ma and AGT-Mi, it decreases for F152I-Mi and F152I-Ma with a rate constant of 0.021 ± 0.001 and 0.028 ± 0.001 min^{-1}, respectively, values in good agreement with those of the slow phase of PMP formation. After 3 h the reaction mixtures containing AGT-Ma, AGT-Mi, F152I-Mi or F152I-Ma were filtered through a Centricon-30 device, and the PMP content of the filtrates were determined by HPLC. The amounts of PMP in AGT-Ma and AGT-Mi filtrates is less than 10% of the original PLP content, whereas that of F152I-Mi and F152I-Ma is about 40% of the original coenzyme content. These data indicate that, unlike for AGT-Ma and AGT-Mi, the overall transamination catalyzed by F152I-Mi and F152I-Ma is characterized by a fast phase that represents the conversion of the mutant from the PLP form to the PMP form followed by a slow phase that could be ascribed to the release of PMP from the enzyme. The last phase is responsible for shifting the PLP-PMP equilibrium toward the PMP form of the mutant. All these data imply that during the overall transamination in the absence of exogenous PLP, either

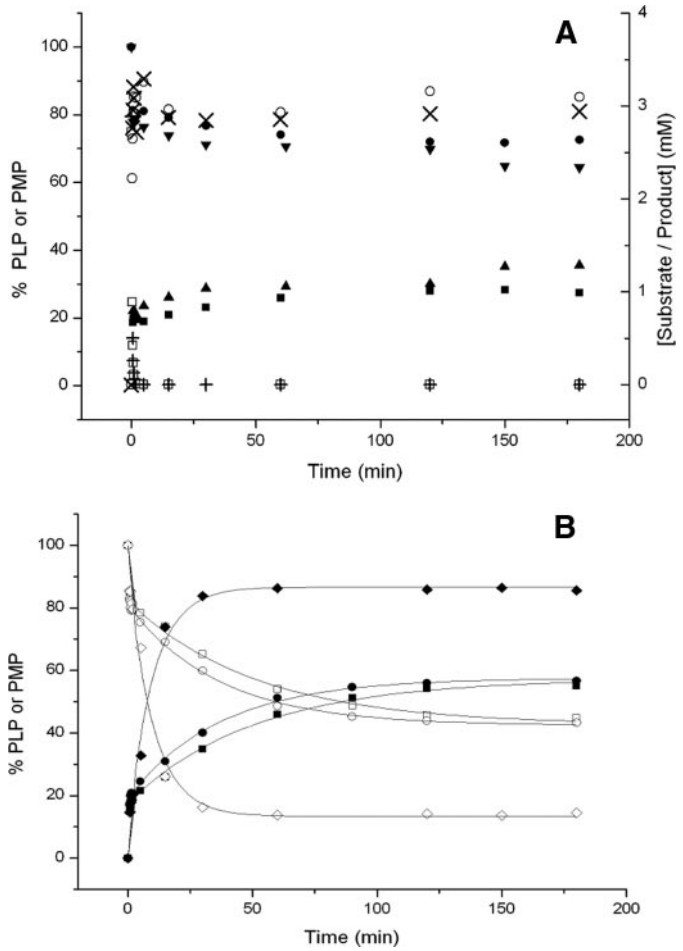

FIGURE 2. **Time course of the overall reaction of AGT-Ma, AGT-Mi, and Phe[152] variants.** AGT-Ma, AGT-Mi, or Phe[152] variants at a concentration of 2.6 μM were incubated at 37 °C in 100 mM potassium phosphate buffer, pH 7.4. At the indicated times, aliquots were withdrawn and denatured. After removal of the precipitated protein by centrifugation, the supernatants were subjected to HPLC analysis as described under "Experimental Procedures." *A*: ●, PLP; ■, PMP; □, glyoxylate; ○, pyruvate, for AGT-Ma; ▼, PLP; ▲, PMP; +, glyoxylate; ×, pyruvate, for AGT-Mi. *B*: □, PLP; ■, PMP for F152I-Mi; ○, PLP; ●, PMP for F152I-Ma; ◇, PLP; ◆, PMP for F152A-Ma. The percentage of PLP or PMP is referred to the original PLP content of the enzymes. The *curves* represent the least-squares fit of a second-order rate equation to the data. The data shown are the means of three independent experiments. In each case, the standard error of the mean was less than 5%.

AGT-Ma or AGT-Mi mainly remain in a coenzyme (PLP or PMP) bound form, *i.e.* in a catalytically competent form, whereas F152I-Mi and F152I-Ma convert into the apo form. This is corroborated by what we observe after 3 h upon adding additional glyoxylate to the reaction mixtures up to a final concentration of 3 mM. Whereas glyoxylate consumption and concomitant pyruvate production for AGT-Ma and AGT-Mi take place with an initial velocity similar to that measured in the presence of the first aliquot of glyoxylate, glyoxylate consumption and concomitant pyruvate production for F152I-Mi and F152I-Ma occur with an initial velocity of about 60% that of the first aliquot. Thus, unlike AGT-Ma or AGT-Mi, F152I-Mi and F152I-Ma need to be continuously supplied with PLP to remain in a catalytically competent form.

Structural Origin of Weak PMP Binding in F152I Mutants—To achieve some insights into the binding mode of PMP and its reduced affinity for the F152I mutants, we decided to model the

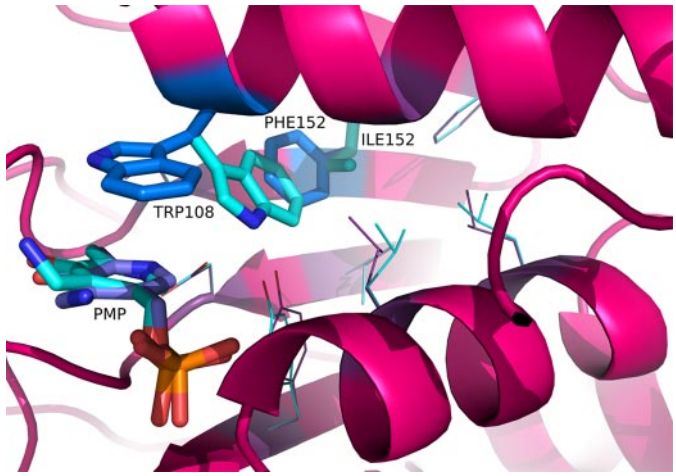

FIGURE 3. **Modeling of the active site of AGT-Ma and F152I variant in the PMP form.** The putative location of Trp[108] at the active site of AGT-Ma and F152I variant in the PMP form is illustrated. Trp[108], Phe[152], and PMP are represented as *blue sticks* in AGT-Ma, whereas Trp[108], Ile[152], and PMP are represented as *cyano sticks* in F152I variant. Oxygen atoms are colored *red*, nitrogen atoms *blue*, and phosphorus *orange*. This figure was rendered using PyMOL (17).

mutated form of AGT, in which Phe[152] was substituted with Ile. Observing the crystal structure of human AGT, we initially noticed that Phe[152] is not directly facing the active site cleft of the enzyme (3) (Fig. 3), being instead located in an adjoining hydrophobic cleft formed by residues Leu[86], Leu[90], Phe[100], Trp[108], Ala[112], Phe[152], Thr[154], Leu[181], Asp[183], and Tyr[204]. Therefore, the observed reduced affinity for PMP in the F152I mutant is probably due to an indirect effect, rather than the direct involvement of Phe[152] in PMP stabilization. A careful inspection of Phe[152] neighboring residues suggested that this indirect effect might be related to the presence of Trp[108], whose side chain engages a stacking interaction with the pyridine ring of PLP and PMP. Indeed, Phe[152] is positioned at a distance of ~5 Å from the C_β atom of Trp[108]. Accordingly, we hypothesized that a misplacement of the Trp[108] side chain, due to the mutation of Phe[152], could account for the decreased affinity for PMP observed for the F152I mutant. This effect might be minimized in the case of the internal aldimine, where PLP is held in position by the Schiff-base forming lysine of the active site.

According to this hypothesis, the replacement of the bulky phenyl moiety of Phe[152] with the side chain of the Ile residue is expected to form a cavity that, in turn, could accommodate the indolic ring of Trp[108]. The presence of this cavity would eventually create a second, stable minimum in the potential energy surface of Trp[108]. To test this hypothesis, we initially performed a quantitative characterization of interior cavities of the wild-type and F152I mutant, focusing on the region comprising Trp[108] and Phe[152]. The wild-type enzyme showed no detectable cavity in this region; on the other hand, the substitution of Phe[152] with Ile generated a cavity, whose dimensions are ~51 Å^3 (~78 Å^2).

Next, because this cavity is adjacent to the side chain of Trp[108], an energy-based prediction of Trp[108] side chain orientation was carried out by rotamer analysis, energy minimization, and molecular dynamics. In the case of the wild-type, the only observed energy minimum (−16.4 kJ/mol) corresponds to

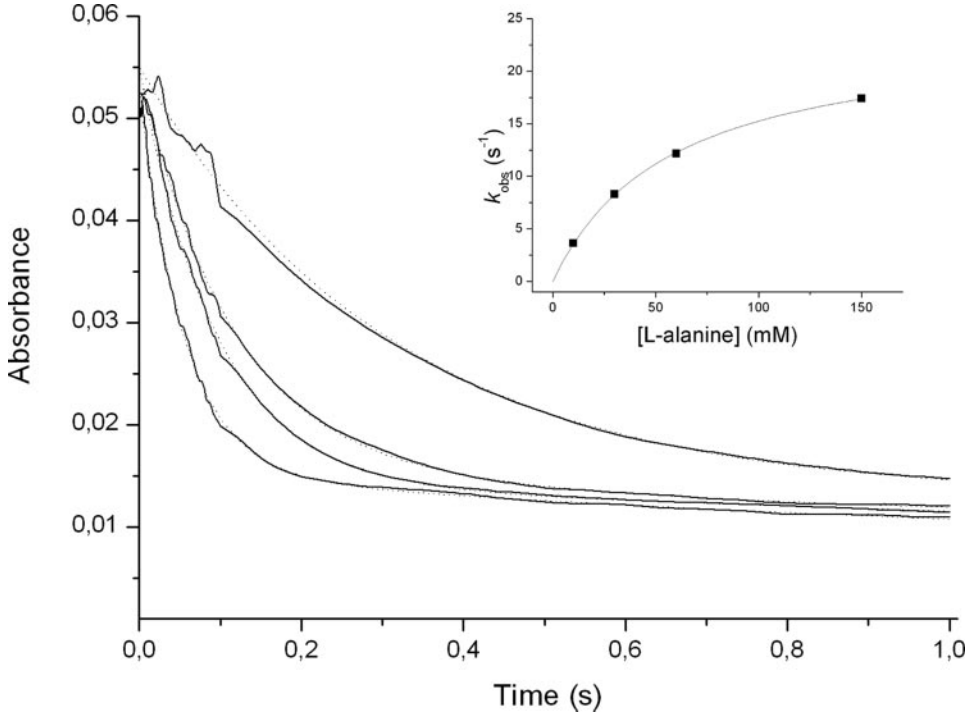

FIGURE 4. **Single wavelength stopped-flow measurements of the reaction of F152A-Ma with L-alanine.** The reaction of F152A-Ma (6 μM) with various concentrations of L-alanine in 100 mM potassium phosphate buffer, pH 7.4, at 25 °C. Time courses at 420 nm are shown. The *dotted lines* are from a fit to Equation 2. The *inset* shows the dependence of the k_{obs} for the decrease of the intensity at 420 nm as a function of L-alanine concentration. The points shown are the experimental values, whereas the *curve* is from the data fitted to Equation 3.

TABLE 3
Transamination half-reaction kinetic parameters of AGT-Ma and F152A-Ma

Enzyme	Half-reaction	k_{max}	K_m^{app}	K_{max}/K_m^{app}
		s^{-1}	mM	$mM^{-1}s^{-1}$
AGT-Ma	E-PLP + L-alanine	49 ± 5[a]	38 ± 9[a]	1.3 ± 0.3[a]
AGT-Ma	E-PMP + glyoxylate	49 ± 1[a]	0.22 ± 0.01[a]	220 ± 11[a]
F152A-Ma	E-PLP + L-alanine	24.0 ± 0.3	57 ± 1	0.42 ± 0.01
F152A-Ma	E-PMP + glyoxylate	60 ± 4	0.30 ± 0.06	200 ± 42

[a] From Ref. 4.

the PLP/PMP stacking conformation, whereas a positive energy value (17.2 kJ/mol) was measured, after energy minimization, in the region accommodating Phe[152]. In the case of the F152I mutant, two energy minima were observed, one corresponding to the native conformation, and the other corresponding to the side chain of Trp[108] turning aside from its original position and partially fulfilling the hydrophobic cavity generated by the absence of the phenyl ring of Phe[152] (Fig. 3). In this case, the measured energy was −3.2 kJ/mol.

Therefore, it can be concluded that the replacement of Phe[152] with a less bulky residue could interfere with the proper positioning of Trp[108], leading to a decreasing affinity of AGT for PMP. According to this model, this effect would be greater if Phe[152] is replaced by alanine. Indeed, we decided to model F152A applying the same procedure used for F152I. A cavity of ~106 Å^3 (~128 Å^2) was identified for the Phe to Ala mutation. Furthermore, this cavity can easily accommodate the phenyl ring of Phe[152], with a negative potential energy of −23.6 kJ/mol. Thus, following this bioinformatic analysis, a binding affinity of F152A for PMP is expected to be lower than that of F152I.

F152A-Ma—To test this hypothesis, the F152A-Ma mutant has been cloned, expressed, and purified. As isolated, F152A mutant contains 2 mol of PLP/dimer and exhibits absorbance and CD spectra in the UV-visible region identical to those of AGT-Ma (data not shown). As shown in Table 2, whereas replacement of Phe[152] by alanine in AGT-Ma does not significantly alter the $K_{D(PLP)}$, it increases by at least ~1400-fold the $K_{D(PMP)}$. Accordingly, the L-alanine half-transamination, characterized by absorbance and CD spectral changes similar to those of F152I-Ma and F152I-Mi, is accompanied by PMP release in an equal amount to ~80% of the original PLP content of the mutant. The time course of the overall transamination catalyzed by F152A, examined under the same experimental conditions described above for wild-type and variants, reaches at 3 h a ratio PMP/PLP of about 6, and is a biphasic process with rate constants of 1.7 ± 0.8 and 0.096 ± 0.008 min^{-1} (Fig. 2*B*). Again, the overall transamination of F152A is characterized by the immediate appearance of a positive dichroic signal at 260 nm, which decreases with a rate constant of 0.141 ± 0.004 min^{-1}, a value in excellent agreement with that of the slow phase of PMP formation. HPLC analysis of the filtrate of the reaction mixture after 3 h reveals the presence of an amount of PMP corresponding to ~70% of the original PLP content. These results indicate that at position 152 alanine, more than isoleucine, impairs the PMP binding affinity and increases the rate of PMP release during the overall transamination reaction. This is consistent with the PMP putative binding mode to Phe[152] variants and validates the bioinformatic analysis.

It should also be pointed out that, although replacement of Phe[152] by alanine on the major allele yielded a fairly active species, it reduces the catalytic efficiency for the pair alanine/glyoxylate to about 30% with respect to AGT-Ma (Table 1). Thus, we tried to understand how the reduced PMP binding affinity could affect the catalytic features of the enzyme. For this purpose, the L-alanine and glyoxylate half-transamination reactions have been recorded by rapid scanning stopped-flow analysis. The rate constant of either the disappearance or the increase of the 420-nm absorbance band shows a hyperbolic dependence on L-alanine (Fig. 4) or glyoxylate concentration, respectively, giving the k_{max}, K_m^{app}, and k_{max}/K_m^{app} values of the half-transamination reactions reported in Table 3. The following considerations could be derived from these data: (i) the catalytic efficiency of L-alanine half-transamination measured under pre-steady state conditions is similar to the value of k_{cat}/K_m measured under steady-state conditions, thus suggest-

TABLE 4
T_m values of AGT-Ma, AGT-Mi and Phe[152] mutants in the holo and apo forms

Enzyme	T_m
	°C
HoloAGT-Ma	76.3 ± 0.8
ApoAGT-Ma	56.6 ± 0.3
HoloAGT-Mi	70.1 ± 1.5
ApoAGT-Mi	51.6 ± 0.3
HoloF152I-Mi	69.9 ± 1
ApoF152I-Mi	45.0 ± 0.1
HoloF152I-Ma	73.6 ± 0.2
ApoF152I-Ma	52.4 ± 0.1
HoloF152A-Ma	66.8 ± 0.2
ApoF152A-Ma	52.1 ± 0.2

ing that, like for AGT-Ma (4), the rate-limiting step of this process for F152A-Ma is the ketimine formation or its hydrolysis, and (ii) the catalytic efficiency of glyoxylate half-transamination in F152A remains almost invariant with respect to that of AGT-Ma, whereas that of L-alanine half-transamination increases about 3-fold, thus providing further support for the role of Phe[152] in selectively stabilizing the AGT-PMP complex.

Thermostability Experiments—Although it is clear that a reduction of PMP binding affinity is one molecular defect shared by the Phe[152] variants, it would be difficult to correlate it with the pathological effect (*i.e.* partial mistargeting to mitochondria) of the F152I mutation encoded on the minor allele. It has been reported that F152I-Mi is sensitive to both proteasomal and trypsin degradation, and that exogenous PLP protects the variant from trypsin digestion (12). These observations together with the recent finding that untagged AGT-Ma in the holo form is significantly more stable than in the apo form (13), and that Phe[152] variants undergo a partial conversion to apoenzyme during the overall transamination, led us to investigate the thermostability of AGT-Ma, AGT-Mi, and F152 variants in both the holo and apo forms. The temperature values of one-half inactivation, T_m, listed in Table 4 merit some comments. First, the T_m values of all these holo enzymatic species are significantly higher than those of the corresponding apoenzymes. The fact that Tyr[260*] and Thr[263*] from one subunit are hydrogen-bonded to the coenzyme phosphate of the other subunit could explain to a certain extent why the holoenzyme is more stable than apoenzyme. Second, the difference in stability between holo and apo is similar for AGT-Ma and AGT-Mi. This is in apparent contrast with what is recently claimed by Hopper *et al.* (5). These authors state that AGT-Ma is stabilized by PLP to a greater extent than AGT-Mi. This apparent contradiction can be understood by considering that the thermal stability, measured by those researchers using an activity-based assay, was not carried out on the holo and apo forms of AGT-Ma and AGT-Mi, but on the major and minor allele enzymes in the presence or absence of exogenous PLP. It is likely that the measurements were made at an enzyme concentration lower than the $K_{D(PLP)}$ of AGT-Ma and AGT-Mi. Thus, in the absence of exogenous coenzyme, AGT-Ma and AGT-Mi could be in the PLP-bound and PLP-unbound forms, whose ratio depends on the enzyme concentration used for the two enzymatic species. This idea is supported by the finding that when the thermostability has been examined using a mass spectrometry-based technique and differential fluorimetry at an enzyme concentration (5 μM) higher than the $K_{D(PLP)}$, a difference in PLP-stabilization degree between AGT-Ma and AGT-Mi could not be observed. Based on our results and the above considerations, it might be reasonable to suggest that the difference in stability between AGT-Ma and AGT-Mi is an intrinsic structural feature of the proteins, due to P11L and I340M polymorphisms. Because Pro[11] belongs to the N-terminal arm, which has been proposed to be involved in the stabilization of the dimer (3), it is possible to suggest that the substitution of Pro[11] by Leu could alter the topology of this region and contribute to destabilization of the dimeric structure.

Finally, and more important, F152I-Mi in the apo form is found to be the more destabilized form among the enzymatic species examined. It is of interest to note that its T_m value is ~6 °C lower than that of apoAGT-Mi. The structural origin of the higher degree of destabilization of apoF152I-Mi with respect to the apo forms of AGT-Mi and F152I-Ma is not easy to explain. However, inspection of the x-ray structure of AGT reveals that helix 5, which has Trp[108] at its N-terminal end, contains residues engaged in several interactions with residues belonging to two random coil regions (residues 235–244 and 258–264) of the adjacent subunit. In particular, Asp[114] and Arg[118] make electrostatic interactions with Lys[236*] and Asp[243*], respectively, Ile[115] makes hydrophobic interaction with Phe[240*], and Arg[111] is hydrogen bonded with the backbone CO of Tyr[260*] and His[261*]. As suggested by bioinformatic analyses, mutation of Phe[152] to Ile generates a cavity in which Trp[108] may be free to move. It is reasonable to suggest that the presence of this cavity could affect the proper positioning not only of Trp[108] but also of some residues of helix 5, thereby compromising the intersubunits contacts. We can speculate that the combined effects of P11L and F152I mutations could result in a synergic destabilization of the dimeric structure of AGT. Moreover the fact that the T_m value of apoF152I-Mi is ~6 °C lower than those of the apoF152-Ma variant supports this view in that it indicates that, although the F152I mutation on its own reduces the PMP binding affinity, it does remarkably interfere with the degree of stabilization of the apoprotein only when associated with the minor allele.

To define if the low T_m value of apoF152I-Mi entails its instability at physiological temperature, the kinetics of thermal inactivation of AGT-Ma, AGT-Mi, and F152I variants has been examined at 37 °C over a period of 3 h. No loss of AGT activity of the holo forms of AGT-Ma, AGT-Mi, F152I-Mi, and F152I-Ma as well as of the apo form of AGT-Ma, AGT-Mi, and F152I-Ma has been observed. In contrast, as shown in Fig. 5, we detected a consistent apoF152I-Mi inactivation, whose extent is dependent on the enzyme concentration. Thus, among the enzymatic species examined, apoF152I-Mi is the most unstable one, susceptible to inactivation at physiological temperature. We then tried to experimentally assess a possible relation between the time-dependent thermal inactivation of apoF152I-Mi and the molecular size of the enzyme. AGT-Ma, AGT-Mi, F152I-Ma, and F152I-Mi in both their holo and apo forms at various enzyme concentrations were incubated at 37 °C, and aliquots withdrawn at time intervals were subjected to gel filtration on a Sephacryl S-300 column. At any time, all enzymatic species elute as dimers. However, whereas the inte-

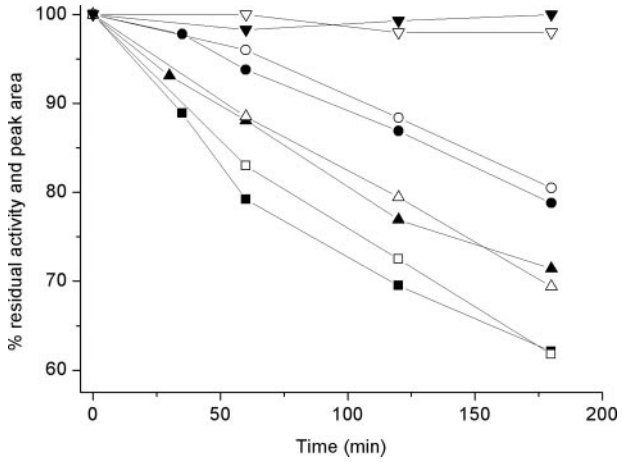

FIGURE 5. **Time-dependent loss of activity and integrated peak area of apoF152i-Mi upon incubation at 37 °C.** ApoF152I-Mi was incubated at 1 (*circles*), 0.5 (*up triangles*), 0.25 μM (*squares*) at 37 °C in 100 mM potassium phosphate buffer, pH 7.4. Aliquots were withdrawn at the indicated times and assayed either for transaminase activity or for the integrated peak areas measured upon gel filtration on a size exclusion chromatography. For comparison, the transaminase activity and the integrated peak area of 0.25 μM apoAGT-Mi upon incubation at 37 °C (*down triangles*) are shown. *Closed* and *open symbols* represent percentage of transaminase activity and integrated peak area, respectively. The *lines* are drawn to guide the eye.

grated peak area of holo- and apoAGT-Ma, holo- and apoAGT-Mi, and holoF152I-Mi remains unchanged, the integrated peak area of apoF152I-Mi decreases as a function of the time of incubation. At various enzyme concentrations the loss of peak area parallels the loss of transaminase activity (Fig. 5). These data strongly suggest that the time-dependent loss of catalytic activity of these enzymatic species could be due to the formation of insoluble high-molecular weight aggregates occurring predominantly at low enzyme concentrations. Considering also that these events are dependent on enzyme concentration, it is reasonable to suggest that (i) as the enzyme concentration of apoF152I-Mi decreases, monomerization occurs, (ii) monomerization of apoF152I-Mi could take place at enzyme concentrations higher than other enzymatic species examined, and (iii) the monomer is more unstable than the dimer, one consequence of which would be aggregation due to artifactual polymerization.

These data demonstrate for the first time that the naturally occurring F152I-Mi variant in the apo form undergoes a significant inactivation at physiological temperature. The *in vivo* functional consequence of this finding could be interpreted as follows. Like many other peroxisomal enzymes, AGT rapidly folds and dimerizes in the cytosol and is imported into peroxisomes in a fully dimeric active state. On the other hand, the mitochondrial import machinery requires proteins to be imported as monomers. The peroxisome-to-mitochondrion mistargeting of AGT in PH1 is due to the combined effects of (i) the generation of a mitochondrial targeting sequence resulting from the P11L polymorphism, and (ii) the presence of monomeric AGT (14). Neither in AGT-Mi nor in F152I-Ma do both of these conditions occur. In contrast, the combined presence of F152I substitution (which appears to interfere with AGT dimerization *in vitro*) and P11L polymorphism take place in F152I-Mi. Thus, in the absence of the saturating PLP concentration, F152I-Mi in a larger percentage than AGT-Mi (and possibly of F152I-Ma, for which no clinical phenotype has been identified until now), could either form aggregates in the cytosol (as observed in our *in vitro* experiments) and/or be imported in mitochondria before having a chance to fold and dimerize. This view is compatible with enzymic phenotype in PH1 patients carrying the F152I mutation. In these patients, a much higher proportion of AGT has been found to redirect away from peroxisomes and toward the mitochondrial matrix than in individuals carrying the minor allelic form (6). Moreover, the fact that when F152I-Mi was expressed in *Escherichia coli* the protein was recovered from the soluble fraction in a lower percentage with respect to AGT-Ma, AGT-Mi, and other Phe[152] variants can be ascribed to its instability and propensity to aggregation.

Although vitamin B6, the precursor of PLP, is known to have a therapeutic effect in PH1 patients carrying the F152I-Mi mutation, up to now it is unclear how this effect is mediated (15, 16). Based on our results, we can propose that the clinical response to the pyridoxine therapy might be due to an increase of PLP concentration in the liver cytosol, thus shifting the equilibrium of F152I-Mi from the apo to the holo form and avoiding monomerization and consequent aggregation and/or mislocation to mitochondria. However, at present any support to this hypothesis is missing.

Conclusions—In summary, in our study evidence has been provided for (i) a role of Phe[152] in selective stabilization of the AGT-PMP complex because, as suggested by bioinformatic analyses, of an indirect effect of this residue mediated by Trp[108], and (ii) a reduced thermostability of the naturally occurring F152I-Mi in the apo form with respect to apoAGT-Mi and apoF152I-Ma. Thus, this biochemical analysis allows us (i) to identify the structural and functional molecular defects of F1521-Mi, (ii) to elucidate the molecular basis of the functional synergism between AGT-Mi and the F152I mutation, and (iii) to speculate on the reason why high doses of pyridoxine could be an effective therapy for PH1 patients harboring the F152I mutation in the minor allele. A similar biochemical approach could be useful to shed light on the molecular defects of other pathogenic variant associated with the minor allele.

REFERENCES

1. Danpure, C. J., Fryer, P., Griffiths, S., Guttridge, K. M., Jennings, P. R., Allsop, J., Moser, A. B., Naidu, S., Moser, H. W., MacCollin, M., and Devino, D. C. (1994) *J. Inherit Metab. Dis.* **17,** 27–40
2. Lumb, M. J., and Danpure, C. J. (2000) *J. Biol. Chem.* **275,** 36415–36422
3. Zhang, X., Roe, S. M., Hou, Y., Bartlam, M., Rao, Z., Pearl, L. H., and Danpure, C. J. (2003) *J. Mol. Biol.* **331,** 643–652
4. Cellini, B., Bertoldi, M., Montioli, R., Paiardini, A., and Borri Voltattorni, C. (2007) *Biochem. J.* **408,** 39–50
5. Hopper, E. D., Pittman, A. M., Fitzgerald, M. C., and Tucker, C. L. (2008) *J. Biol. Chem.* **283,** 30493–30502
6. Danpure, C. J., Purdue, P. E., Fryer, P., Griffiths, S., Allsop, J., Lumb, M. J., Guttridge, K. M., Jennings, P. R., Scheinman, J. I., Mauer, S. M., and Davidson, N. O. (1993) *Am. J. Hum. Genet.* **53,** 417–432
7. Danpure, C. J., and Jennings, P. R. (1988) *Clin. Sci.* (*Lond.*) **75,** 315–322
8. Cellini, B., Bertoldi, M., and Borri Voltattorni, C. (2003) *FEBS Lett.* **554,** 306–310
9. Bertoldi, M., and Borri Voltattorni, C. (2000) *Biochem. J.* **352,** 533–538
10. Dundas, J., Ouyang, Z., Tseng, J., Binkowski, A., Turpaz, Y., and Liang, J. (2006) *Nucleic Acids Res.* **34**, W116–W118
11. Bohm, G., Muhr, R., and Jaenicke, R. (1992) *Protein Eng.* **5,** 191–195

12. Coulter-Mackie, M. B., and Lian, Q. (2008) *Mol. Genet. Metab.* **94,** 368–374
13. Cellini, B., Montioli, R., Bianconi, S., Lopez-Alonso, J. P., and Voltattorni, C. B. (2008) *Protein Pept. Lett.* **15,** 153–159
14. Leiper, J. M., Oatey, P. B., and Danpure, C. J. (1996) *J. Cell Biol.* **135,** 939–951
15. Monico, C. G., Olson, J. B., and Milliner, D. S. (2005) *Am. J. Nephrol.* **25,** 183–188
16. Monico, C. G., Rossetti, S., Olson, J. B., and Milliner, D. S. (2005) *Kidney Int.* **67,** 1704–1709
17. De Lano, W. (2002) *The PyMol Molecular Graphics System*, DeLano Scientifics, San Carlos, CA